metals

MDPI

Article

Recent Advances in Creep Modelling Using the θ Projection Method

William Harrison

Department of Mechanical Engineering, Faculty of Science and Engineering, Swansea University, Swansea SA1 8EN, UK; w.harrison@swansea.ac.uk

Abstract: The theta projection method has been used to predict uniaxial creep curve shapes for a wide range of materials. However, one of the criticisms of the existing method is that the multilinear approach, commonly used to correlate theta parameters to applied test conditions, does not extrapolate well over a full range of creep conditions, due to not accounting for changes in creep mechanisms. This is particularly important for evaluating the creep behaviour of structural engineering components that operate in an environment in which a wide range of stress and/or temperatures exist during their service life. This study uses the theta projection method to evaluate creep curves for the nickel-based superalloy, Waspaloy, over a range of test conditions, considering changes in observed dominant creep mechanisms. A clear break in the trend of θ_3 and θ_4 with respect to stress is observed, indicating that a change in mechanism is important for tertiary creep. Using a power law approach along with optimisation algorithms, the residual error between predicted and experimentally observed creep curves is reduced. With more accurate prediction of creep curves, creep rates throughout the duration of creep can be more accurately calculated, providing the basis of more accurate computational creep models.

Keywords: creep; superalloys; theta projection method

Citation: Harrison, W. Recent Advances in Creep Modelling Using the θ Projection Method. *Metals* **2024**, *14*, 1395. https://doi.org/10.3390/met14121395

Academic Editor: Babak Shalchi Amirkhiz

Received: 11 October 2024
Revised: 19 November 2024
Accepted: 21 November 2024
Published: 5 December 2024

1. Introduction

Engineering components that operate at high temperatures for extended periods of time, such as those in high-temperature plant applications or aeroengines, must be designed to withstand the effects of creep deformation and rupture. Single-point prediction methods can provide useful estimations of stress rupture lives, but for many applications, characterising the evolution of creep rate over time is important. This is the case for applications where stress relaxation occurs around stress concentration features. Full creep curve methods such as the theta (θ) projection method [1] and the Omega method [2] describe the evolution of creep rate from primary creep through the minimum creep rate to tertiary creep. Other methods include a true stress model by Wu [3] which has a similar formulation to the θ method but includes terms for micromechanical deformation, and an extension to the Wilshire method [4,5].

The θ projection method correlates creep strain, ε_t, to time, t, using

$$\varepsilon_t = \theta_1\left(1 - e^{-\theta_2 t}\right) + \theta_3\left(e^{\theta_4 t} - 1\right) \quad (1)$$

where θ_{1-4} are the θ coefficients. θ parameters are obtained from experimental observations by minimising the error between Equation (1) and constant stress creep data. θ_1 and θ_2 characterise primary creep, whereas θ_3 and θ_4 characterise tertiary creep. These parameters can be correlated with applied stress and temperature to predict creep curves for any applied conditions. This is commonly achieved through use of the following multilinear expression [6]:

$$ln(\theta_k)_j = a_k + b_k\sigma_j + c_k T_j + d_k\sigma_j T_j \qquad j = 1,\ldots,n\,, \quad k = 1,\ldots,4 \quad (2)$$

where σ_j and T_j are applied stress and temperature for n number of tests. Soares [7] recently modified this multilinear expression to include terms for $1/T$ and $ln(1/T)$, and applied the θ projection method to accurately predict compressive creep in a refractory material. This multilinear approach interpolates well over the range of creep data it is correlated over. However, it does not inherently extrapolate well and gives non-zero values for θ_{1-4} when both stress and temperature are zero. Alternatively, a power law approach has been adopted [8]:

$$\theta_k = A_k \left(\frac{\sigma_h}{\sigma_{TS}} \right)^{n_k} \exp\left(\frac{-Q_k^*}{RT_h} \right) \qquad k = 1, \ldots, 4 \tag{3}$$

where A_k and n_k are material constants, R is the universal gas constant, and Q_k^* is the activation energy for θ_k. Here, the stress for each set of test data, σ_j, is normalised by the tensile stress, σ_{TS}, at the applied test temperature, T_j. For $k = 1$ and $k = 3$, the effects of temperature ae compensated for by normalising stress by σ_{TS} and Q_1^* and Q_3^* are equal to zero.

The θ projection method has been successfully used to evaluate the creep properties of P92 steel [9], Inconel-625 [10], austenitic stainless steels [11,12], and the titanium alloy Ti-6.2.4.6. [13]. A constitutive model for creep based on the theta projection method was developed by Evans [6]. This method used the θ parameters to characterise evolving creep in terms of dislocation hardening, dislocation recovery, and internal material damage, and was developed into a finite element-based model to predict creep in notched bars. This model has further been used to predict creep deformation and rupture in a TiAl alloy during the small punch creep test [14]. This constitutive model has also been used to predict creep in non-constant applied conditions, showing improved predictions over strain-hardening- and time-hardening-based models for Waspaloy [15]. Law et al. [16] also used a finite element model based on the theta projection method to evaluate the stress in a cylindrical pressure vessel wall. Results using this method compared favourably to simulations based on Norton's power law. Song et al. [17] proposed a modified theta method for 12Cr1MoV steel, using a logarithmic form as opposed to the exponential form of Equation (1); however, the fitting process was the same.

Many creep-resistant alloys exhibit different creep behaviour over a wide range of applied conditions. The changes in deformation behaviour have been documented in the form of deformation mechanism maps by Ashby et al. [18,19]. These maps split the stress/temperature domain into discrete regions bound by lines where the contribution of adjoining mechanisms is considered the same. Gray and Whittaker [20] described this region splitting in various steels and the importance of considering it when modelling creep life. The reasons for different observed behaviours can be attributed to different dominant creep mechanisms. This was emphasised in Grade 22 steel tube (2.25Cr-1Mo) where three distinct regions of creep were observed in data for creep lives of ~50 to ~100,000 h [21]. Whittaker et al. [22] described this change in behaviour in 316H stainless steel over a wide range of stresses, attributing the change in behaviour above and below the yield stress; Esposito et al. [23] later confirmed similar behaviour in the same steel, attributing the transition in observed behaviour to a transition between dislocation- and diffusion-based creep mechanisms. These transitions in creep behaviour have also been observed in the titanium alloys Ti-834 [24] and Ti-45Al-2Mn-2Nb [25].

In nickel-based superalloys such as Waspaloy, different creep behaviour has been observed at stresses above and below the yield stress, σ_Y. This different behaviour has been confirmed by differences in the evolution of dislocation structures observed by TEM [26] and EBSD [27]. Wu [28] described different mechanisms of creep in terms of kinetics of dislocation mobility for dislocation glide (IDG), dislocation climb (IDC), and grain boundary sliding (GBS). The inherent different rates of these mechanisms result in the dominant creep mechanism being dependent on applied conditions. A true stress model based on this approach has been successfully applied to Waspaloy [3] as well as other alloys such as Haynes 282 [29], Alloy 800 [30], and 9Cr-1Mo steel [31].

2. Materials

Creep data were obtained from constant stress uniaxial creep tests described by Evans [6] and later Wilshire and Scharning [32]. The composition of the Waspaloy alloy used is given in Table 1. The alloy was solution-annealed at 1353 K for 4 h then water-quenched, followed by heat treatment at 1123 K for 4 h then air-cooling and at 1033 K for 16 h then air-cooling. This gave the superalloy a microstructure consisting of equiaxed grains with an average diameter of 45 µm and $\gamma\prime$ particles with an average diameter of 0.3 µm. Constant stress creep tests were conducted over a temperature range of 600–750 °C and a stress range of 200–1150 MPa, giving a range of specimen creep lives from <1 h to >3000 h.

Table 1. Chemical composition (wt.%) of Waspaloy used for this study (Adapted from [6]).

Element	**Cr**	**Co**	**C**	**Mn**	**Si**	**Fe**	**Mo**	**Ti**	**Al**	**B**	**Zr**
wt%	19.1	13.5	0.03	0.10	0.10	0.79	4.08	3.18	1.30	0.005	0.07
Element	**S**	**P**	**Cu**		**Ag**	**Pb**		**Bi**		**Ni**	
wt%	0.0025	0.01	0.10		5 ppm	10 ppm		0.5 ppm		Bal.	

3. Model Details

3.1. Initial Fitting of θ Parameters

The first step of the fitting process was to normalise the experimental creep curves by time to rupture, t_F, and rupture strain, ε_F. Then, normalised θ parameters were obtained for each normalised creep curve by minimising the squared error between the strain at each data point and that predicted by Equation (1). A Newton–Raphson iterative method was used to find the minimum of

$$\phi = \sum_{j=1}^{n} \{\varepsilon_j - \theta_1[1 - exp(\theta_2 t_j)] - \theta_3[exp(\theta_4 t_j)] - 1\} \quad (4)$$

where ε_j represents the normalised strain values for each data point, j, and t_j is the normalised time. Due to accelerated creep rates caused by the onset of localised necking towards the end of the creep tests, some curves were truncated by up to 10% of specimen rupture life, corresponding to an accelerating creep rate. This occurred automatically within the optimisation procedure if a better fit could be obtained by removing the last data point iteratively, until the best fit was found.

The Newton–Raphson method does not require calculation of the Hessian matrix [33]; however, values on the diagonal of the inverted Hessian were obtained to find the variance of the final values of θ_{1-4}. These values of variance for each θ parameter give a measure of the quality of fit and are equal to the standard deviation squared. Standard deviations for the four theta parameters, $\sigma_{SD,1-4}$, are given in subsequent graphs.

Once optimum values for θ_{1-4} and $\sigma_{SD,1-4}$ are obtained, these are converted to real values by multiplying by maximum creep strain (in the case of θ_k and $\sigma_{SD,k}$, $k = 1, 3$) or dividing by maximum time (in the case of θ_k and $\sigma_{SD,k}$, $k = 2, 4$).

Example fits are shown in Figure 1, and theta values obtained using this method, along with standard deviations, are shown in Figures 2–5.

3.2. Correlating θ Parameters to Applied Conditions

Obtaining θ parameters from experiments allows creep curves to be regenerated, but the real value in the method comes from correlating the θ parameters to applied test conditions (stress and temperature). This allows creep rates at other test conditions to be predicted and is an important step towards building a computer model for creep deformation. Previous studies [6,7] have used either a multilinear fit (Equation (2)) or a power law approach (Equation (3)) to correlate θ_{1-4} to applied stress and temperature.

This study uses the latter power law approach. Since the creep strain calculated using Equation (1) is sensitive to changes in each θ parameter, once each parameter has been correlated, the others must be re-evaluated using the method described in Section 3.1. Since creep is dominated by tertiary creep, the rate parameter θ_4 was correlated to applied conditions first, followed by θ_2, then θ_3, and finally θ_1.

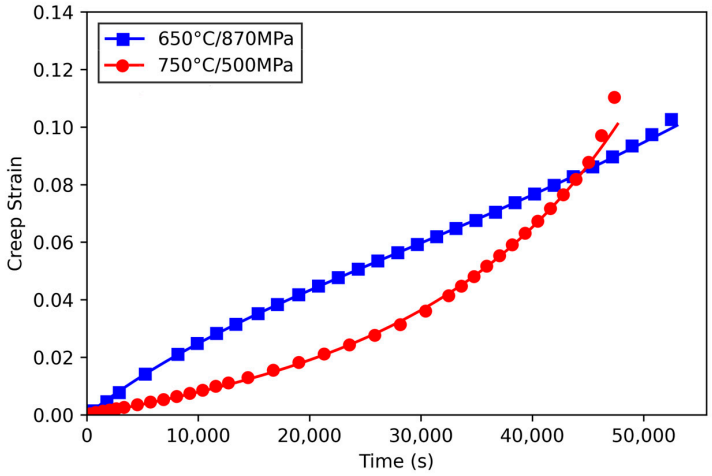

Figure 1. Example creep curves for Waspaloy with points representing experimental data and lines representing fits using Equation (1).

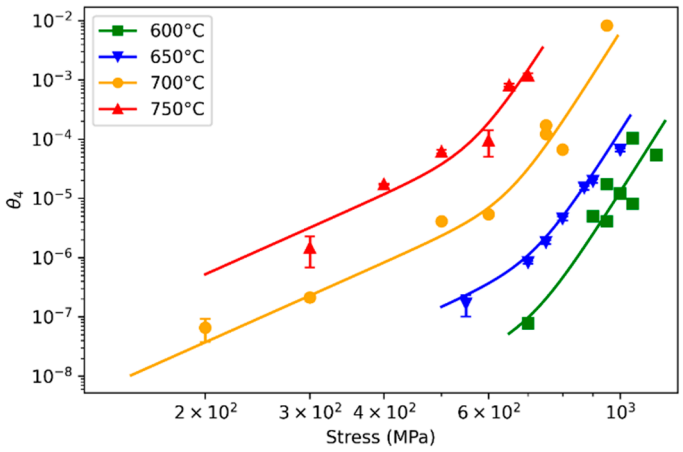

Figure 2. The variation of θ_4 with stress for each T with lines of fit obtained using Equation (6).

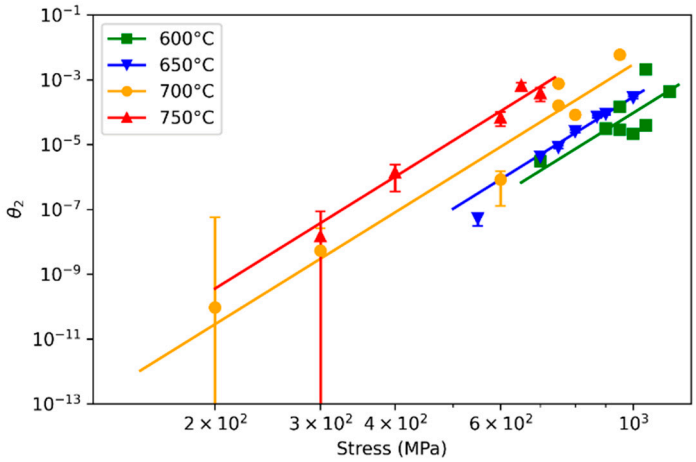

Figure 3. The variation of θ_2 with stress for each T with lines of fit obtained using Equation (8).

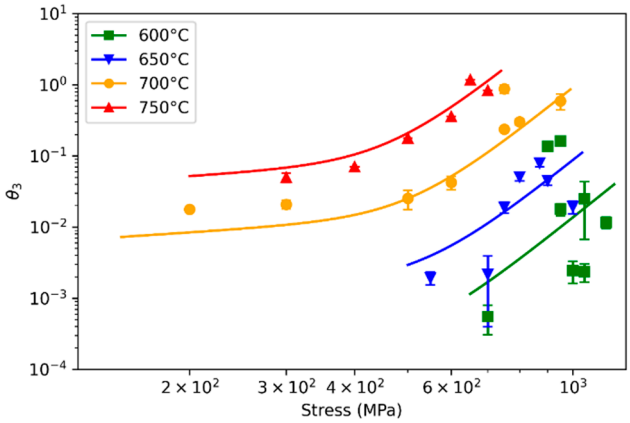

Figure 4. The variation of θ_3 with stress for each T with lines of fit obtained using Equation (9).

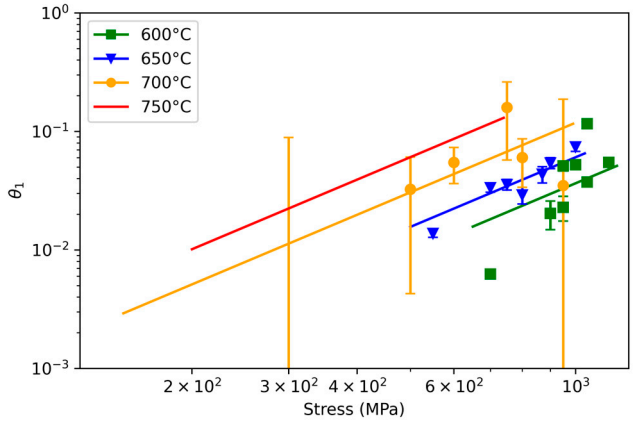

Figure 5. The variation of θ_1 with stress for each T with lines of fit obtained using Equation (10).

Comparing $\ln(\theta_4)$ to $\ln(\sigma/\sigma_{TS})$ does not give a single linear trend for temperatures of 600 °C to 750 °C, as shown in Figure 2. Instead, the gradient increases from ~4.5 to ~16 as stress increases, indicating a change in dominant creep mechanism at different applied test conditions. This phenomenon is well documented in Waspaloy and different micromechanisms have been characterised by TEM [26] and EBSD [27]. More recently, Evans et al. [34] used an artificial neural network (ANN) methodology to evaluate changes in activation energy and, hence, mechanism over different levels of strain in the same alloy. These studies identified different activation energies for different creep regimes. Using a similar approach and assuming that the different mechanisms are independent of each other, the following expression can be used to correlate θ_k to σ and T :

$$\theta_k = \sum_{h=1}^{m} \left\{ A_{k,h} \left(\frac{\sigma}{\sigma_{\mathrm{TS}}} \right)^{n_{k,h}} \exp\left(\frac{-Q^*_{k,h}}{RT} \right) \right\} \qquad h = 1, \ldots, m, \quad k = 1, \ldots, 4 \tag{5}$$

where m is the number of creep mechanisms. $A_{h,k}$ and $n_{h,k}$ are the constants that define the correlation between θ_k and σ for each theta value, k, and mechanism, h. $Q^*_{h,k}$ correlates to temperature, T. For θ_4, the following equation can be used to correlate θ_4 to σ and T:

$$\theta_4 = A_{4,1} \left(\frac{\sigma}{\sigma_{\mathrm{TS}}} \right)^{n_{4,1}} \exp\left(\frac{-Q^*_{4,1}}{RT} \right) + A_{4,2} \left(\frac{\sigma}{\sigma_{\mathrm{TS}}} \right)^{n_{4,2}} \exp\left(\frac{-Q^*_{4,2}}{RT} \right) \tag{6}$$

where two independent mechanisms exist. A similar form of the equation was proposed by Johnson, Henderson, and Khan [35] where the minimum creep rate, $\dot{\varepsilon}_{\min}$, comprises two power law terms:

$$\dot{\varepsilon}_{\min} = \left[A_1 \left(\frac{\sigma}{\sigma_0} \right)^{n_1} + A_2 \left(\frac{\sigma}{\sigma_0} \right)^{n_2} \right] \tag{7}$$

where A_1 and n_1 are the material constants for one mechanism and A_2 and n_2 are the constants for a second mechanism. σ_0 is a reference stress such as yield stress, σ_{PS}. Once θ_4 has been correlated to applied conditions, θ_{1-3} are re-evaluated using Equation (4), supplementing θ_4 with Equation (4). Next, θ_2 is correlated with applied test conditions. For the range of applied conditions, primary creep contributes less to the total creep strain than tertiary creep. Therefore, more scatter is observed for θ_2 than θ_4. Comparing $\ln(\theta_2)$ to $\ln(\sigma/\sigma_{TS})$ gives a single linear trend:

$$\theta_2 = A_{2,1} \left(\frac{\sigma}{\sigma_{\mathrm{TS}}} \right)^{n_{2,1}} \exp\left(\frac{-Q^*_{2,1}}{RT} \right) \tag{8}$$

This process is then repeated for θ_3 and θ_1, using Equations (9) and (10), respectively. Since two creep mechanisms have been identified for tertiary creep, θ_3 is correlated to σ and T using

$$\theta_3 = A_{3,1} \left(\frac{\sigma}{\sigma_{\mathrm{TS}}} \right)^{n_{3,1}} \exp\left(\frac{-Q^*_{3,1}}{RT} \right) + A_{3,2} \left(\frac{\sigma}{\sigma_{\mathrm{TS}}} \right)^{n_{3,2}} \exp\left(\frac{-Q^*_{3,2}}{RT} \right) \tag{9}$$

Finally, θ_1 is correlated to σ and T using

$$\theta_1 = A_{1,1} \left(\frac{\sigma}{\sigma_{\mathrm{TS}}} \right)^{n_{1,1}} \exp\left(\frac{-Q^*_{1,1}}{RT} \right) \tag{10}$$

The values obtained using these initial fits are shown in Table 2. Plots of θ_{1-4} are shown in Figure 2, along with correlations using Equations (6) and (8)–(10). Since primary creep was insignificant at 750 °C, θ_1 was difficult to characterise. This is shown by the lack of data points for this temperature in Figure 5. Similarly, at 700 °C low levels of primary creep resulted in a low confidence of fit for θ_1 resulting in high standard deviations being observed at this temperature in the same figure. For θ_3 and θ_4, a smooth transition between different creep regimes is observed as opposed to the sharp transitions observed in previous work [36,37]. Using these correlations, creep curves can be predicted for any given uniaxial conditions. Alternatively, times to specified levels of creep strain can be plotted for a wide range of test conditions. Figure 6 shows times to 0.5%, 1.0%, 2.0%, and 5.0% strain, predicted using this method. A correlation plot for experimental and predicted times to 2.0% strain is given in Figure 7. It can be seen that although a reasonable fit is achieved, the correlations at the higher temperatures can be improved.

Table 2. Parameters obtained from initial fit ($k = 1, \ldots, 4$).

θ_k	$Q^*_{k,1}$	$n_{k,1}$	$A_{k,1}$	$Q^*_{k,2}$	$n_{k,2}$	$A_{k,2}$
	(J·mol^{-1})		**(MPa)**	**(J·mol^{-1})**		**(MPa)**
θ_1	59,900.2	1.952	184.931	0.0	0.0	0.0
θ_2	106,856.9	11.468	1207.185	0.0	0.0	0.0
θ_3	287,233.3	0.5	4.86×10^{13}	222,840.5	6.230	7.02×10^{11}
θ_4	315,215.1	4.465	3.6×10^{12}	250,611.0	15.914	1.21×10^{11}

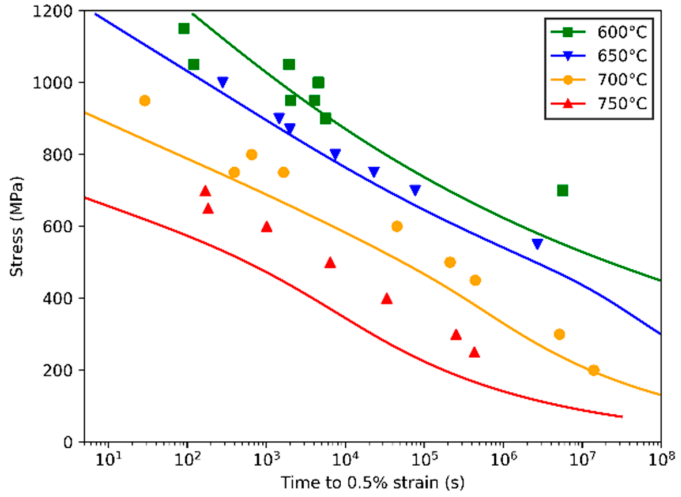

(**a**)

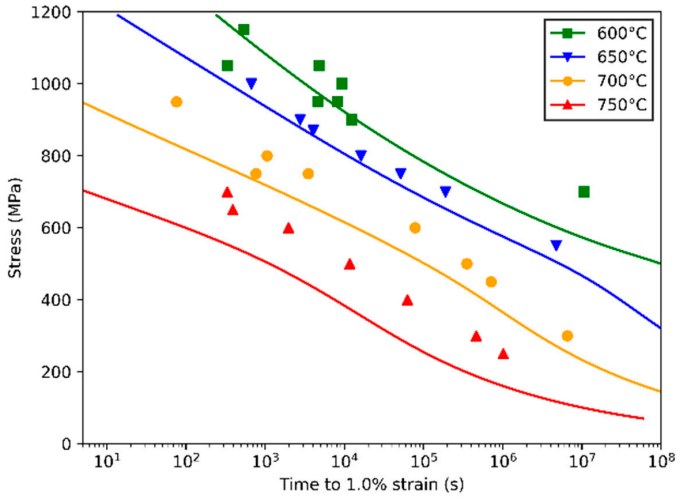

(**b**)

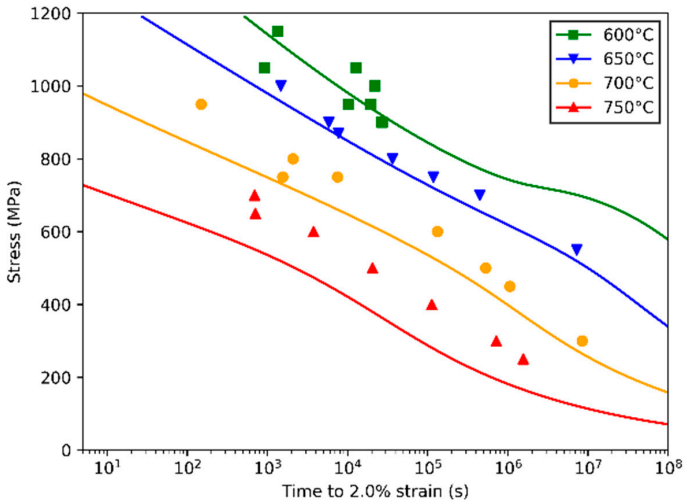

(**c**)

Figure 6. *Cont.*

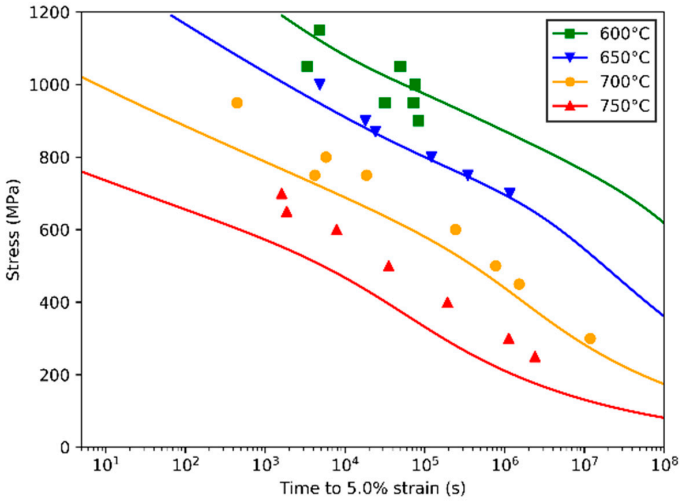

(**d**)

Figure 6. Times to (**a**) 0.5%, (**b**) 1.0%, (**c**) 2.0%, and (**d**) 5.0% creep strain with predictions obtained using parameters given in Table 2.

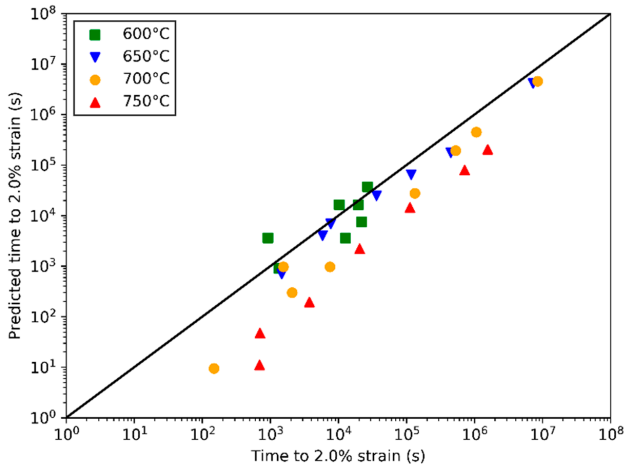

Figure 7. Correlation plot for experimental and predicted times to 2.0% creep strain using parameters given in Table 2.

3.3. Optimising θ Parameters

The correlations between experimental times to strain and those predicted by the theta method can clearly be improved. The correlation can be improved by fine tuning the parameters $A_{k,h}$, $n_{k,h}$, and $Q^*_{k,h}$* to minimise the difference between model fits and experimental data. To achieve this, an error measure (or loss function) between the data and model fits must be defined. Due to the exponential nature of time, across the range of data, a loss function based on stress was used. Also, due to different numbers of data points at different temperatures, a mean error was taken for datasets at each temperature. This avoids overfitting to one temperature at the detriment of fitting to data at a temperature with few data points. Various loss functions have been proposed for regression analysis and each have different advantages and disadvantages. Mean absolute error (MAE) and mean squared error (MSE) are both commonly used, with the latter placing more emphasis on outlying data points. MAE was used due to the stochastic nature of creep date and the loss function was defined as

$$MAE = \frac{1}{n}\sum_{j=1}^{n}\left|\frac{\sigma_j}{\sigma_{TS}} - \frac{\hat{\sigma}_j}{\sigma_{TS}}\right| \quad (11)$$

where n is the number of tests at each test temperatures, σ_j is the stress for the jth test, $\hat{\sigma}_j$ is the predicted stress for the jth test, and σ_{TS} is the tensile strength at test temperature. This error measure was used as the dependent variable in a non-linear regression analysis to find the optimum fit with $A_{k,h}$, $n_{k,h}$, and $Q^*_{k,h}$ ($k = 1, \ldots, 4$, $h = 1, 2$) as the independent variables. The Python-based optimisation and root finding module scipy.optimize was used and, where applicable, bounds of +/−10% of initial values were used since the initial fits were considered to be close to the final solution. Four different non-linear optimisation algorithms were used: the Nelder–Mead (Simplex) algorithm, Powell's conjugate direction method (Powell) [38], a conjugate gradient algorithm (CG), and sequential quadratic programming (SLSQP). The resulting mean absolute errors along with information on time taken to find solutions for each algorithm are given in Table 3.

Table 3. Optimisation results for each algorithm.

Method	MAE	Function Evaluations	Iterations
Simplex	3.198	12,605	10,000
Powell	3.316	9948	19
CG	3.384	3645	43
SLSQP	3.392	362	13

The Powell, CG, and SLSQP algorithms all reached minima within 50 iterations. However, the Nelder–Mead method had not found a minimum error at the limit of 10,000 iterations which equated to 12,605 function evaluations. However, the Nelder–Mead (Simplex) method resulted in the lowest final error, despite not meeting the convergence criterion. Due to the number of independent variables, the number of function evaluations is high for the Simplex- and gradient-based methods; however, because the initial values are close to optimum, the Simplex method can search for a solution with high fidelity. The optimum values for $A_{k,h}$, $n_{k,h}$, and $Q^*_{k,h}$ ($k = 1, \ldots, 4$, $h = 1, 2$) obtained using the Simplex algorithm are given in Table 4. Predictions of time to strain using each method are shown in Figure 8a–d.

Table 4. Parameters obtained from optimised fit using the Simplex algorithm (k = 1, . . ., 4).

θ_k	$Q^*_{k,1}$	$n_{k,1}$	$A_{k,1}$	$Q^*_{k,2}$	$n_{k,2}$	$A_{k,2}$
	(J·mol^{-1})		(Mpa)	(J·mol^{-1})		(Mpa)
θ_1	52,710.1	2.109	200.52	0.0	0.0	0.0
θ_2	111,381.7	13.524	1074.05	0.0	0.0	0.0
θ_3	300,973.2	0.480	5.05×10^{13}	264,380.9	5.916	6.92×10^{11}
θ_4	311,327.7	4.728	3.42×10^{12}	274,952.9	15.506	1.29×10^{11}

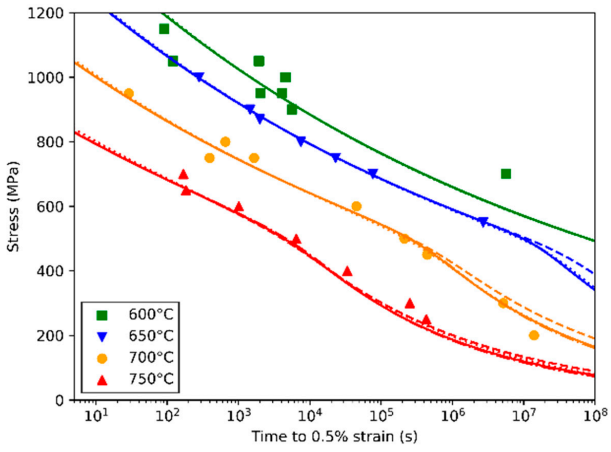

(**a**)

Figure 8. *Cont.*

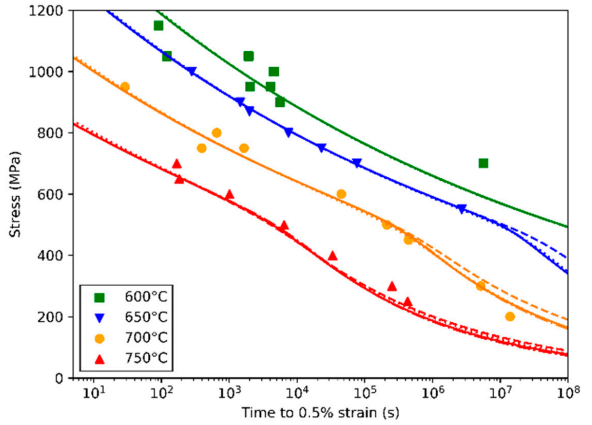

(**b**)

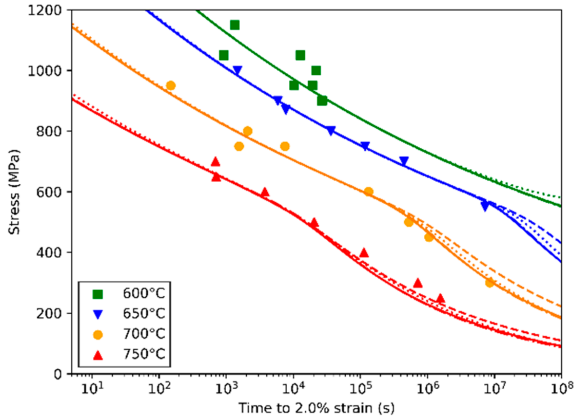

(**c**)

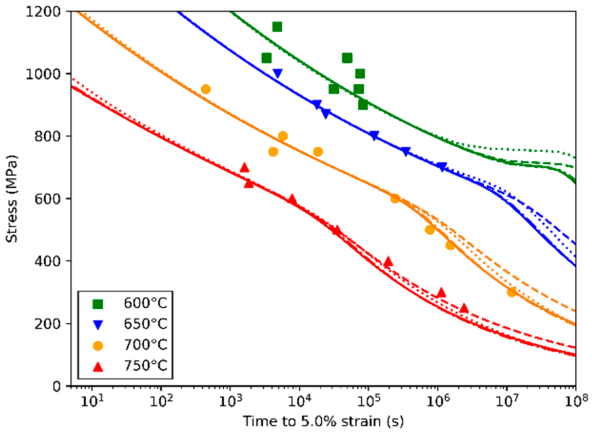

(**d**)

Figure 8. Times to (**a**) 0.5%, (**b**) 1.0%, (**c**) 2.0%, and (**d**) 5.0% creep strain with predictions obtained using each optimisation algorithm. Solid lines show predictions using the Simplex algorithm (parameters given in Table 4), dotted lines show predictions using the values obtained from the Powell algorithm, dot/dashed lines show predictions using CG method, and dotted lines show the SLSQP method.

Comparing predicted times to strain against those obtained experimentally shows that the fit is much better than the original fit shown in Figure 7. A correlation plot for times to 2.0% strain, comparing experimental values to those predicted using the Simplex method, is given in Figure 9.

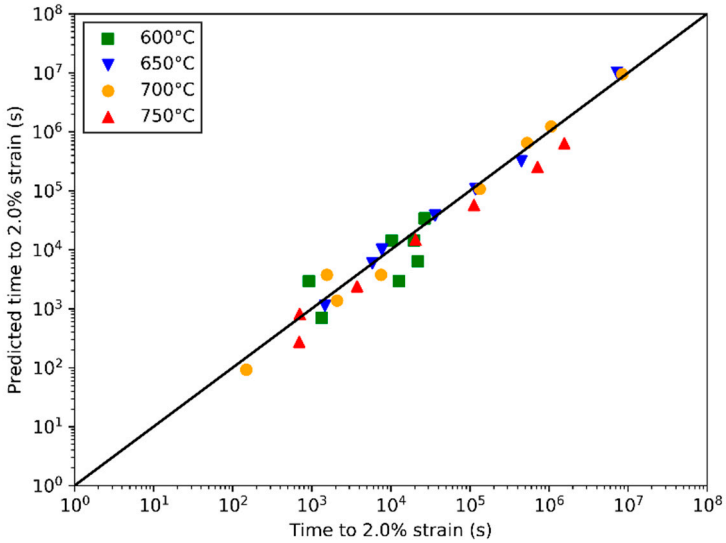

Figure 9. Correlation plot for experimental and predicted times to 2.0% creep strain using parameters given in Table 3.

4. Discussion

Previous research has shown that the micromechanism of creep in nickel-based superalloys is dependent on applied conditions. Whittaker et al. [26] showed that at lower stresses in Waspaloy, the rate of dislocation movement is controlled by dislocation climb at $\gamma\prime$ precipitates. At higher stresses, the formation of dislocation networks has more influence on rate due to forest hardening. Later, Birosca et al. [27] determined the role of grain boundaries during creep at different applied stresses for the same alloy. The clear break in creep behaviour displayed while fitting parameters to the θ projection method follows these previous findings. Also, since the break in behaviour is only displayed for θ_3 and θ_4, this provides further evidence that this is a phenomenon effecting tertiary creep.

The values of $Q^*_{k,h}$ obtained for θ_3 and θ_4, both in the high- and low-stress regime, are in the range of 264.4 and 311.3 KJ/mol. These values are comparable to the activation energy for self-diffusion in polycrystalline nickel of 292 KJ/mol obtained by MacEwan et al. [39]. Wilshire and Scharning [32] obtained a value of activation energy for creep of ∼276 KJ/mol. Since creep in particle-strengthened alloys occurs by diffusion-controlled dislocation mechanisms such as climb, it can be expected that the activation energies for creep and self-diffusion are similar. Wu et al. [3] proposed three different mechanisms for creep in Waspaloy: grain boundary sliding (GBS), dislocation glide (DXNG), and dislocation climb (DXNC). The activation energies for these mechanisms were given as 300.8 kJ/mol, 424.0 kJ/mol, and 337.2 kJ/mol, respectively. The activation energies obtained in this study are close to those obtained for GBS and DXNC; however, multiple mechanisms may occur concurrently. Whittaker et al. [26] found activation energies of 420 kJ/mol for creep at stresses above the yield stress and 340 kJ/mol for creep at lower stresses. This study found that at higher stresses, the activation energy $Q^*_{k,h}$ was lower, with values of $Q^*_{3,1}$ = 264.4 KJ/mol and $Q^*_{4,1}$ 275.0 KJ/mol dominant at higher stresses and $Q^*_{3,2}$ = 301.0 KJ/mol and $Q^*_{4,1}$ = 311.3 KJ/mol dominant at lower stresses. The method used for this study does not specify a break point in terms of stress; however, this can be calculated by the intersection of lines on a $\ln(\theta_k)$ vs. $\ln(\sigma/\sigma_{TS})$ plot. Since $Q^*_{k,h}$ varies for the high- and low-stress regions, the value of $\ln(\sigma/\sigma_{TS})$ at which the lines intersect will vary with time. Calculating this change in break point for θ_4 shows that the value of σ/σ_{TS} increases from ∼0.85 at 600 °C to ∼0.91 at 750 °C. Since σ_{TS} decreases with temperature, the stress corresponding to a transition in creep behaviour decreases from 986.9 MPa at 600 °C to 755.8 MPa at 750 °C. This is shown in Figure 10.

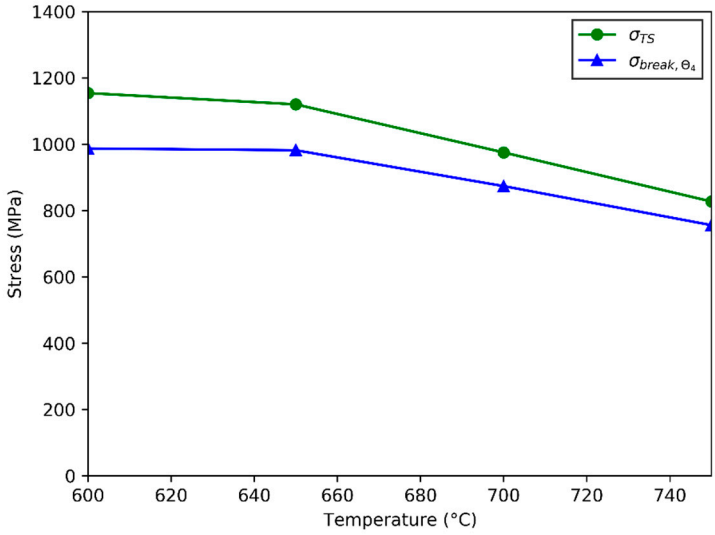

Figure 10. Stresses corresponding to a change in dominant creep behaviour predicted using Equation (6) and parameters given in Table 3.

One of the advantages in not explicitly stating the break point is that the predictions have a smooth transition between different creep regimes. This is an advantage when models are prepared for use in computational models where stresses may transition between different regions of creep behaviour.

The values of activation energy obtained are strongly dependent on the value used to normalise the stress. For this study, σ_{TS} values were taken from a previous study [32]. More recently, Evans [40] proposed the use of maximum stress, σ_{max}, to normalise σ as better predictions of minimum creep rates are obtained. The value of σ_{max} is greater than σ_{TS}. The scatter observed at 600 °C could be a source of error for calculating activation energy.

5. Conclusions

This paper introduces a modification to the theta (θ) projection method whereby the correlation of θ_{1-4} to stress and temperature includes a transition in dominant creep behaviour as stress increases, a phenomenon observed when predicting rupture lives and minimum creep rates in previous studies. This transition in dominant behaviour, characterised by a different set of model parameters, only occurs for θ_3 and θ_4, indicating that this phenomenon effects tertiary creep only. The form of the equations includes a smooth transition between two independent creep mechanisms, without the need to explicitly define a 'break' point.

The parameters for the model were optimised using an error measure based on mean absolute error between model predictions and experimental values of stress for each creep test. The Simplex-based optimisation algorithm produced the best improvement in model fit despite taking the longest to run.

The activation energies obtained from this study were comparable to those obtained for stress rupture lives and minimum creep rates for Waspaloy from previous studies with all values close to the activation energy for self-diffusion in the nickel alloy matrix (292 KJ/mol). With different activation energies obtained for the different regions of creep, the transition from one set of model parameters did not occur at a single σ or σ/σ_{TS} for all temperatures. Instead, the transition from one region to another increased from $\sim$0.85 σ/σ_{TS} at 600 °C to $\sim$ 0.91σ/σ_{TS} at 750 °C.

The research has shown that although the θ projection method is a phenomenological model, the relationships between stress, temperature, and time vary as the dominant mechanism of creep varies. This allows more accurate predictions of creep rate over a wide range of creep conditions, providing the basis for improved computational creep models, using techniques such as finite element analysis.

Funding: This research received no external funding.

Data Availability Statement: The original contributions presented in the study are included in the article, further inquiries can be directed to the corresponding author.

Conflicts of Interest: The author declares no conflicts of interest.

References

1. Evans, R.W.; Parker, J.D.; Wilshire, B. An Extrapolation Procedure for Long Term Creep-Strain and Creep Life Prediction. *Proc. Recent Adv. Creep Fract. Eng. Mater. Struct.* **1982**, *135*, 135–184.
2. Prager, M. Development of the MPC Omega Method for Life Assessment in the Creep Range. *J. Press. Vessel Technol.* **1995**, *117*, 95–103. [CrossRef]
3. Wu, X.; Williams, S.; Gong, D. A True-Stress Creep Model Based on Deformation Mechanisms for Polycrystalline Materials. *J. Mater. Eng. Perform.* **2012**, *21*, 2255–2262. [CrossRef]
4. Wilshire, B.; Battenbough, A.J. Creep and creep fracture of polycrystalline copper. *Mater. Sci. Eng. A* **2007**, *443*, 156–166. [CrossRef]
5. Harrison, W.; Whittaker, M.; Williams, S. Recent advances in creep modelling of the nickel base superalloy, Alloy 720Li. *Materials* **2013**, *6*, 1118–1137. [CrossRef]
6. Evans, R.W. A constitutive model for the high-temperature creep of particle-hardened alloys based on the θ projection method. *Proc. R. Soc. London. Ser. A Math. Phys. Eng. Sci.* **2000**, *456*, 835–868. [CrossRef]
7. Soares, T.R.L.; Kieliba, I.; Azenha, M.; Tonnesen, T.; Lourenço, P.B. A theta projection model for compressive creep behaviour of refractories at high temperature: Application to alumina-spinel. *Meccanica* **2023**, *58*, 2401–2420. [CrossRef]
8. Harrison, W.; Abdallah, Z.; Whittaker, M. A model for creep and creep damage in the γ-titanium aluminide Ti-45Al-2Mn-2Nb. *Materials* **2014**, *7*, 2194–2209. [CrossRef]
9. Liu, H.; Peng, F.; Zhang, Y.; Li, Y.; An, K.; Yang, Y.; Zhang, Y.; Guan, X.; Zhu, W. A New Modified Theta Projection Model for Creep Property at High Temperature. *J. Mater. Eng. Perform.* **2020**, *29*, 4779–4785. [CrossRef]
10. Kumar Krovvidi, S.C.S.P.; Vanaja, J.; Christopher, J.; Goyal, S.; Das, C.R.; Bhaduri, A.K. Creep Behavior of Inconel-625 and Its Modeling at 843 K. *Trans. Indian Natl. Acad. Eng.* **2022**, *7*, 541–548. [CrossRef]
11. Jeyaraj, A.; Vijayanand, V.D.; Ganesan, V.; Ravindran, D.; Reddy, G.V.P.; Sankaran, S.; Mannan, S.L. Grain Size Effect on Creep Properties of 304HCu SS and Modelling of Creep Curves Using Modified Theta Projection Approach. *Trans. Indian Natl. Acad. Eng.* **2022**, *7*, 635–643. [CrossRef]
12. Ruban, R.; Latha, S.; Sivapirakasam, S.P.; Srinivasan, V.S.; Prasad Reddy, G.V. On new relation for theta projection approach for the prediction of creep behaviour of alloy D9I austenitic stainless steel. *Mater. Today Proc.* **2019**, *46*, 9154–9158. [CrossRef]
13. Evans, M. The θ projection method and small creep strain interpolations in a commercial Titanium alloy. *J. Mater. Sci.* **2001**, *36*, 2875–2884. [CrossRef]
14. Lancaster, R.J.; Harrison, W.J.; Norton, G. Materials Science & Engineering A An analysis of small punch creep behaviour in the γ titanium aluminide Ti–45Al–2Mn–2Nb. *Mater. Sci. Eng. A* **2015**, *626*, 263–274. [CrossRef]
15. Harrison, W.J.; Whittaker, M.T.; Deen, C. Creep behaviour of Waspaloy under non-constant stress and temperature. *Mater. Res. Innov.* **2013**, *17*, 323–326. [CrossRef]
16. Law, M.; Payten, W.; Snowden, K. Finite element analysis of creep using Theta projection data. *Int. J. Press. Vessel. Pip.* **1998**, *75*, 437–442. [CrossRef]
17. Song, M.; Xu, T.; Wang, Q.; Wang, W.; Zhou, Y.; Gong, M.; Sun, C. A modified theta projection model for the creep behaviour of creep-resistant steel. *Int. J. Press. Vessel. Pip.* **2018**, *165*, 224–228. [CrossRef]
18. Ashby, M.F. A first report on deformation-mechanism maps. *Acta Metall.* **1972**, *20*, 887–897. [CrossRef]
19. Frost, H.J.; Ashby, M.F. *Deformation-Mechanism Maps: The Plasticity and Creep of Metals and Ceramics*; Pergamon Press: Elmsford, NY, USA, 1982.
20. Gray, V.; Whittaker, M. The changing constants of creep: A letter on region splitting in creep lifing. *Mater. Sci. Eng. A* **2015**, *632*, 96–102. [CrossRef]
21. Whittaker, M.T.; Harrison, W.J. Evolution of Wilshire equations for creep life prediction. *Mater. High Temp.* **2014**, *31*, 233–238. [CrossRef]
22. Whittaker, M.T.; Evans, M.; Wilshire, B. Long-term creep data prediction for type 316H stainless steel. *Mater. Sci. Eng. A* **2012**, *552*, 145–150. [CrossRef]
23. Esposito, L.; Bonora, N.; De Vita, G. Creep modelling of 316H stainless steel over a wide range of stress. *Procedia Struct. Integr.* **2016**, *2*, 927–933. [CrossRef]
24. Abdallah, Z.; Perkins, K.; Williams, S. Advances in the Wilshire extrapolation technique—Full creep curve representation for the aerospace alloy Titanium 834. *Mater. Sci. Eng. A* **2012**, *550*, 176–182. [CrossRef]
25. Abdallah, Z.; Whittaker, M.T.; Bache, M.R. High temperature creep behaviour in the γ titanium aluminide Ti–45Al–2Mn–2Nb. *Intermetallics* **2013**, *38*, 55–62. [CrossRef]
26. Whittaker, M.; Harrison, W.; Deen, C.; Rae, C.; Williams, S. Creep deformation by dislocation movement in waspaloy. *Materials* **2017**, *10*, 61. [CrossRef]

27. Birosca, S.; Liu, G.; Ding, R.; Jiang, J.; Simm, T.; Deen, C.; Whittaker, M. The dislocation behaviour and GND development in a nickel based superalloy during creep. *Int. J. Plast.* **2019**, *118*, 252–268. [CrossRef]
28. Wu, X. *Deformation and Evolution of Life in Crystalline Materials*; Taylor & Francis: London, UK, 2019.
29. Ding, Y.P.; Wu, X.J.; Liu, R.; Zhang, X.Z.; Khelfaoui, F. Creep performance characterization for Haynes 282TM using the deformation-mechanism-based true stress model. *Therm. Sci. Eng. Prog.* **2023**, *37*, 101603. [CrossRef]
30. Wu, X.J. Comment on "Theoretical and Experimental Study of Creep Damage on Alloy 800 at High Temperature (MSA 140953)". *Mater. Sci. Eng. A* **2021**, *820*, 141543. [CrossRef]
31. Zhang, X.Z.; Wu, X.J.; Liu, R.; Liu, J.; Yao, M.X. Deformation-mechanism-based modeling of creep behavior of modified 9Cr-1Mo steel. *Mater. Sci. Eng. A* **2017**, *689*, 345–352. [CrossRef]
32. Wilshire, B.; Scharning, P.J. Theoretical and practical approaches to creep of Waspaloy. *Mater. Sci. Technol.* **2009**, *25*, 242–248. [CrossRef]
33. Yang, X.-S. Chapter 20—Numerical Methods. In *Engineering Mathematics with Examples and Applications*; Yang, X.-S., Ed.; Academic Press: Cambridge, MA, USA, 2017; pp. 231–241, ISBN 978-0-12-809730-4.
34. Evans, M.; Williams, T. Assessing the capability of the Wilshire equations in predicting uniaxial creep curves: An application to Waspaloy. *Int. J. Press. Vessel. Pip.* **2019**, *172*, 153–165. [CrossRef]
35. Johnson, A.E.; Henderson, J.; Khan, B. Paper 26: Multiaxial Creep-Strain/Complex-Stress/Time Relations for Metallic Alloys with Some Applications to Structures. In Proceedings of the Institution of Mechanical Engineers, Conference Proceedings; SAGE Publications: London, UK; 1963; pp. 2–27.
36. Whittaker, M.T.; Wilshire, B. Long term creep life prediction for Grade 22 (2·25Cr-1Mo) steels. *Mater. Sci. Technol.* **2011**, *27*, 642–647. [CrossRef]
37. Whittaker, M.T.; Wilshire, B. Creep and Creep Fracture of 2.25Cr–1.6W Steels (Grade 23). *Mater. Sci. Eng. A* **2010**, *527*, 4932–4938. Available online: http://linkinghub.elsevier.com/retrieve/pii/S0921509310004302 (accessed on 10 October 2024). [CrossRef]
38. Powell, M.J.D. An efficient method for finding the minimum of a function of several variables without calculating derivatives. *Comput. J.* **1964**, *7*, 155–162. [CrossRef]
39. MacEwan, J.R.; MacEwan, J.U.; Yaffe, L. Self-Diffusion in Polycrystalline Nickel. *Can. J. Chem.* **1959**, *37*, 1623–1628. [CrossRef]
40. Evans, M. The Important Role Played by High-Temperature Tensile Testing in the Representation of Minimum Creep Rates Using S-Shaped Curve Models. *Metall. Mater. Trans. A* **2023**, *54*, 4796–4805. [CrossRef]